Computer Simulation of Phase Separation in Binary Polymer Mixtures

TAKAAKI MATSUOKA* and SATORU YAMAMOTO

Toyota Central Research and Development Laboratories, Incorporated, 41-1, Aza, Yokomichi, Oaza Nagakute, Nagakute-cho, Aichi-gun, Aichi 480-11, Japan

SYNOPSIS

Phase separation of binary polymer mixtures was numerically simulated by solving the time-dependent Langevin equation with Flory–Huggins free energy in two dimensions by using a finite difference method. Spinodal decomposition following structure coarsening was calculated. Simulation results were verified by evaluating the evolution of the wave number obtained from the calculated phase structure by Fourier transformation. Then, computer experiments were carried out to investigate effects of volume fraction and polymer characters, the number of segments, and solubility parameter on morphology. The phase separation time, when the phase began to separate, decreased with deviating volume fraction from 0.5 and with decreasing number of segments and difference between solubility parameters. The difference between solubility parameters had the largest influence on the phase separation time among them and had two effects, the acceleration of phase separation and the restriction of structure coarsening. © 1995 John Wiley & Sons, Inc.

INTRODUCTION

Polymer mixtures, called polymer alloys and blends, are very attractive as structural and functional materials because of their variable properties. A lot of polymer alloys and blends have been developed in polymer industries and are commercially available for practical products now. Because it is well known that their variable properties are caused by morphology or phase structure, then the morphological study is important to develop polymer alloys and blends. Experimental studies of phase separation and morphology were made by digital image analysis[1] and light scattering.[2,3] Numerical simulations of phase separation were performed to investigate spinodal decomposition of polymer system by Monte Carlo method.[4–7]

The dynamics of concentration fluctuations are phenomenally described by the time-dependent Langevin equation. Cahn and Hilliard first developed a diffusion equation for spinodal decomposition,[8] and Cook added thermal fluctuations to the equation.[9] Petschek and Metiu applied the Ginzburg–Landau model to numerical simulation of spinodal decomposition in two dimensions by using a finite difference method.[10] They discussed that the results of simulations appropriated to the spinodal decomposition of a two-component mixture on the probability of the concentration and the structure function. Chakrabarti et al. presented a numerical study of the dimensionless Cahn–Hilliard model without a thermal fluctuation term for late stages of spinodal decomposition in three-dimensional binary system and showed that the late-time behavior of the system was described in terms of scaling with a characteristic length.[11] Ariyapadi et al. predicted the domain size in polymer blends during phase separation by solving a modified form of the Cahn–Hilliard equation, in which the mobility was described as a function of the concentration.[12] Chen et al. performed a computer simulation of early-stage spinodal decomposition of polymer solutions in two-dimensional Fourier space considering composition-dependent mobility and diffusivity.[13] These previous studies indicate that the Cahn–Hilliard–Cook equation can be used for the prediction of phase separation in binary polymer systems.

* To whom correspondence should be addressed.

Journal of Applied Polymer Science, Vol. 57, 353–362 (1995)
 CCC 0021-8995/95/030353-10

In practical usage, we are interested in the effect of polymer characters on phase separation and structure because phase structures are different from polymer to polymer. However, the relation between polymer characters and the phase separation and structure is not discussed so far. In this article, relations of the number of segments, solubility parameter, and volume fraction with the phase separation and structure were investigated in binary polymer systems by computer simulation.

THEORY AND NUMERICAL METHODS

Phase Separation Model

The time evolution of concentration fluctuation in the spinodal decomposition is described by the nonlinear Langevin equation.

$$(\partial\phi/\partial t) = M\nabla^2(\delta F/\delta\phi) + \eta(\mathbf{r}, t) \quad (1)$$

where $\phi(\mathbf{r}, t)$ is the order parameter related to the concentration of one of components, $F(t)$ is the free-energy functional, $\eta(\mathbf{r}, t)$ is the thermal noise, M is the constant mobility, t is the time, and $\mathbf{r}$ is the spatial position vector. The thermal noise plays a role in the early stage of phase separation but does not affect the phase structure in the late stage. Because the interest of this article is taken in the late stage of phase separation, the noise term is neglected.

The free-energy functional is assumed to be given by the Ginzburg–Landau expansion.

$$F(t) = k_B T \int d\mathbf{r}[(1/2)K(\nabla\phi)^2 + (1/2!)(\partial^2 f/\partial c^2)\phi^2 + (1/4!)(\partial^4 f/\partial c^4)\phi^4] \quad (2)$$

where k_B is Boltzmann's constant, $f(c)$ is the free-energy density, T is the temperature, and K is the gradient energy parameter. For polymers, K is given by:[14]

$$K = a^2/(18c_1c_2) \quad (3)$$

where c is the concentration ($c_1 + c_2 = 1$) and subscripts 1 and 2 denote polymer 1 and polymer 2, respectively. a is the characteristic length related to the segment size s:[15]

$$a = [s_1^2c_1 + s_2^2c_2]^{1/2} \quad (4)$$

Substituting eq. (2) into eq. (1), the time-dependent Ginzburg–Landau equation is obtained as follows:

$$(\partial\phi/\partial t) = k_B TM\nabla^2[-b\phi + u\phi^3 - K(\nabla\phi)^2] \quad (5)$$

where

$$b = (\partial^2 f/\partial c^2) \quad (6)$$

$$u = (\partial^4 f/\partial c^4) \quad (7)$$

The free-energy density of a binary polymer mixture is given by the Flory–Huggins lattices theory:

$$f(c) = (c_1/N_1)\ln(c_1) + (c_2/N_2)\ln(c_2) + \chi c_1c_2 \quad (8)$$

where, $c = c_2$, N is the number of segments and χ is the interaction parameter. From eqs. (6), (7), and (8), b and u become:

$$b = -1/(N_1c_1) - 1/(N_2c_2) + 2\chi \quad (9)$$

$$u = (\tfrac{1}{3})[1/(N_1c_1^3) + 1/(N_2c_2^3)] \quad (10)$$

The concentration is given from the order parameter:

$$c = (\phi/\phi_e + 1)/2 \quad (11)$$

where

$$\phi_e = (b/u)^{1/2} \quad (12)$$

In the late stage, order parameters approach ϕ_e or $-\phi_e$ in the region except boundary of domains.

Assuming that T, M, b, u, and K are constant, eq. (5) becomes the following dimensionless equation in a simple fashion:[11]

$$(\partial\psi/\partial\tau) = (1/2)\nabla^2(-\psi + \psi^3 - \nabla^2\psi). \quad (13)$$

where

$$\gamma = (b/K)^{1/2}\mathbf{r} \quad (14)$$

$$\psi = (u/b)^{1/2}\phi \quad (15)$$

$$\tau = (2k_B TMb^2/K)t \quad (16)$$

Polymer Characters

Polymer characters required for obtaining coefficients b, u, and K are the number of segments N, segment size s, and interaction parameter χ. Assuming that the monomer is defined as a segment, these parameters are estimated by the following relations.

$$N = M_w/M_u \tag{17}$$

$$s = (r_0/M^{1/2})M_u^{1/2} \tag{18}$$

$$\chi = (v/RT)(\delta_A - \delta_B)^2 \tag{19}$$

$$v = M_u/\rho \tag{20}$$

where, M_w is the weight-averaged molecular weight, M_u is the molecular weight of monomer, $r_0/M^{1/2}$ is the mean-square end-to-end distance, v is the molar volume of solvent, R is the gas constant, δ is the solubility parameter, and ρ is the density. We can get these values of polymers from literature.[16]

Calculations

Equations (5) and (13) were numerically solved in two dimensions by using a finite difference method for dimension and dimensionless cases, respectively. The time derivative is approximated by the forward differential scheme. Computations were carried out using two-dimensional 128 × 128 lattice grid with periodic boundary conditions. It was assumed that two components are solved each other at the initial time and then quenched in an immiscible region. The initial concentrations were chosen to be randomly distributed between −0.01 and +0.01 (the average of the fluctuation equals 0) at the average concentration or volume fraction because of the neglect of the thermal noise.

Calculation conditions are summarized in Table I. The characters of polymer 1 were defined as a standard model polymer with $N = 5000$, $s = 0.5$ nm, $v = 50$ cm^3/mol, and $\delta = 9$ (cal/cm^3)$^{1/2}$, which were nearly extracted from characters of polypropylene. Effects of the number of segments, solubility parameter, and volume fraction of polymer 2 on morphology were investigated by numerical experiments. For one computing run, only one of the condition parameters was changed from each standard value underlined in the table. The segment length and the molar volume were constant because they were unique to the polymer. The standard condition was a symmetric system with $\Delta\delta = 1$, where $\Delta\delta$ is the difference of solubility parameters between polymers 1 and 2.

Fourier Transformation

The time evolution of the phase separation is usually studied by a light scattering experiment. It was reported that the power spectrum of two-dimensional Fourier transform of the phase structure image is equivalent to the scattering intensity.[1] To verify the simulation, the calculated phase structure was analyzed by the fast Fourier transformation and then compared with experimental results. The Fourier transform of $L \times L$ two-dimensional data is described as:

$$F_{jk} = \sum_{n=1}^{L}\sum_{m=1}^{L} \psi_{nm} \cdot W^{(n\cdot j + m\cdot k)};$$

$$j = 1, 2, \cdots L; k = 1, 2, \cdots L \tag{21}$$

$$W = \exp(-2\pi i/L) \tag{22}$$

The power spectrum of the Fourier transform, P, is obtained by the following:

$$P_{jk} = (A_{jk}^2 + B_{jk}^2)^{1/2} \tag{23}$$

where A and B are the real part and imaginary part of the Fourier transform, respectively. The average power spectrum of wave number q is expressed by:

$$P_q = \sum_{q-1/2<q\leqq q+1/2} P_{jk} \Big/ \sum_{q-1/2<q\leqq q+1/2} 1 \tag{24}$$

$$q = [(j-1)^2 + (k-1)^2]^{1/2} \tag{25}$$

The reduced wave number Q_m and the reduced time τ' are defined as follows:

Table I Calculation Conditions

		Polymer 1	Polymer 2					
N	[−]	5000	12	50	100	500	1000	5000
v	[cm^3/mol]	50	50					
s	[nm]	0.5	0.5					
δ	[(cal/cm^3)$^{0.5}$]	9.0	9.2	9.3	9.5	10.0	10.5	
f_v	[−]	$1 - f_v$	0.2	0.3	0.4	0.5		

N: number of segments, v: molar volume, s: segment size. δ: solubility parameter, f_v: volume fraction of polymer 2, underlined; standard values.

$$Q_m(\tau') = q_m(\tau')/q_m(\tau' = 0) \quad (26)$$

$$\tau' = \tau/\tau_s \quad (27)$$

where, q_m is the wave number at which the intensity shows the peak of the power spectrum and τ_s is the scaling parameter for fitting the time scale to the light scattering results.

RESULTS

Phase Structures

Calculated results of phase structures during phase separation are shown in Figure 1 in the dimensionless scale for a volume fraction of 0.3. The results are obtained by solving eq. (13). The scale bar indicates the concentration of polymer 2. Therefore, white and black mean polymers 1 and 2, respectively. In gray areas, polymer 2 is solved in polymer 1 at the concentration indicated with the scale bar. At the initial time, the whole area is uniformity painted with half-bright gray because the concentration fluctuation is very small, about an average concentration of 0.3. Increasing time, the fluctuation increases, although the morphology does not change visibly until a dimensionless time of 10. After that, the phase separation occurs at the time between 10 and 100 and then a droplet/matrix type phase structure clearly appears. Polymer 2 becomes droplets in the matrix of polymer 1 because the volume fraction of the former is less than that of the latter. The coalescence coarsening is observed with time.

Also, phase structures for volume fraction 0.5 are shown in Figure 2. The phase separation begins at an earlier time than that of volume fraction 0.3. The morphology is a fine percolated type and is coarsening as it is after that. The boundary between polymers 1 and 2 is distinct. Figure 3 shows the phase structure for volume fraction 0.7. The morphology is the droplet/matrix type like that for volume fraction 0.3. However, the components are altered like the droplets as polymer 1 and the matrix as polymer 2.

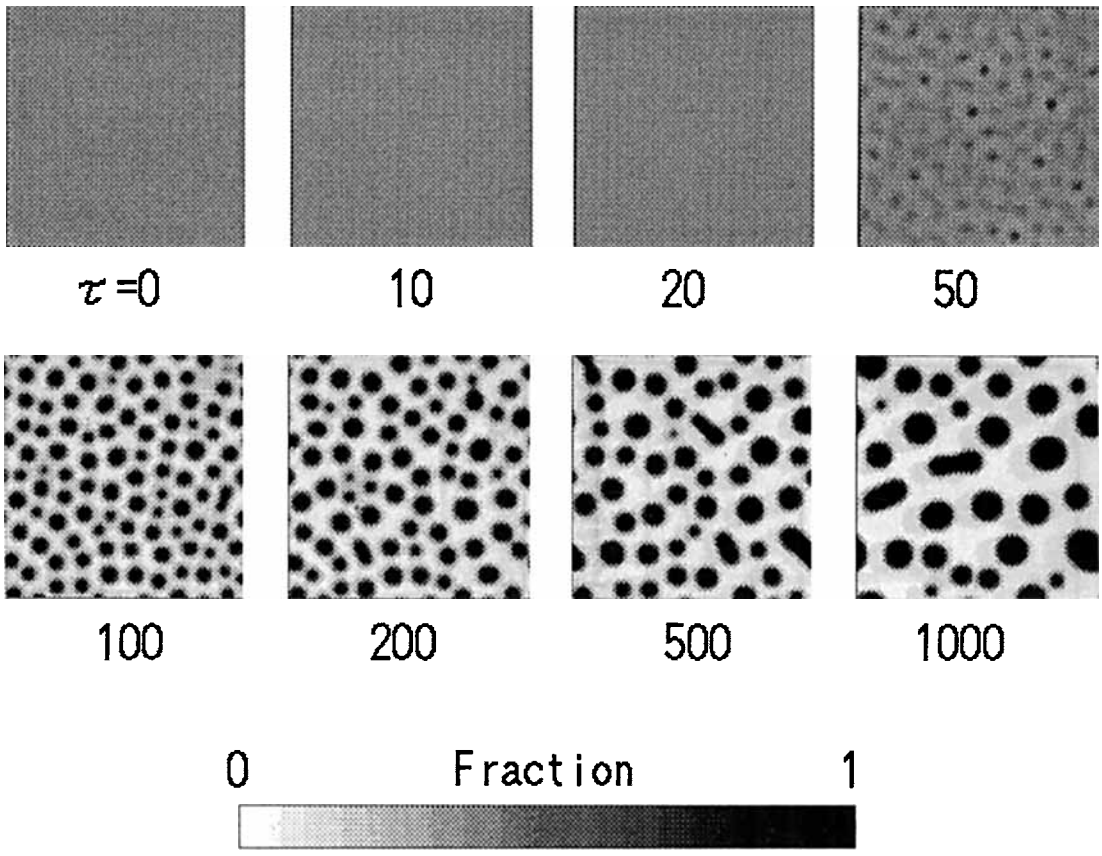

Figure 1 Phase structures during phase separation for volume fraction 0.3 in dimensionless scale.

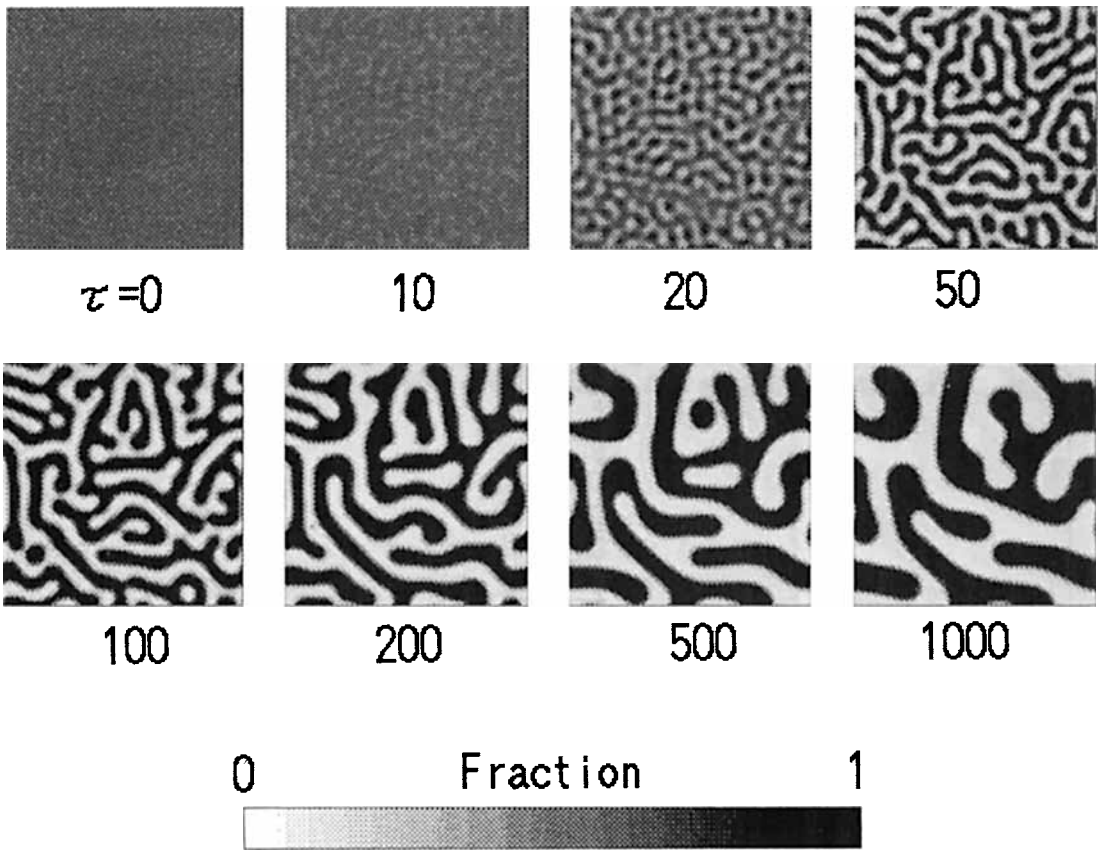

Figure 2 Phase structures during phase separation for volume fraction 0.5 in dimensionless scale.

Time Evolution of Wave Number

The Fourier transform images for volume fraction 0.5 are shown in Figure 4. A circle profile appears in each phase structure except the initial one (refer to Fig. 2). It is called the spinodal ring. The ring diameter decreases with time. Figure 5 shows the intensity against the wave number or the time evolution of the power spectrum. The peak of intensity increases with time. On the other hand, the wave number q_m decreases with time because of the coarsening of the structure. The time evolution of the reduced wave number is shown in Figure 6, comparing with the experimental one.[3] As shown in the figure, we were able to find one scaling parameter τ_s to fit the calculated results to the experimental ones. This indicates that the calculation was made successfully.

Effects of Polymer Characters

The statistical dispersion, $\Phi = \langle\phi^2\rangle - \langle\phi\rangle^2$, is shown in Figure 7 as a function of a dimensionless time, $t^* = k_B TMt$, for the change of volume fraction f_v. Where, $\langle\rangle$ means average, and the results are obtained by solving eq. (5). The results for volume fractions 0.6 and 0.7 are almost same as those of 0.4 and 0.3, respectively. There is no phase separation when $f_v \leqq 0.2$ or $f_v \geqq 0.8$. The phase separation time, which is defined as a time when Φ rises up rapidly from zero, is delayed with decreasing and increasing volume fraction from 0.5. The curve is shifted in the time direction by changing volume fraction.

Figure 8 shows the effect of the number of segments N. The phase separation time increases with decreasing the number of segments. The evolution of Φ is, however, not so changed when $N > 100$. To avoid the phase separation, the number of segments must be less than 20, which means that one of the mixture components must be oligomer not polymer. It is noted that the time is a dimensionless number defined as $t^* = k_B TMt$. The mobility is assumed to be constant in the calculation, but it actually depends on the number of segments. Decreasing the number of segments, the mobility increases and then the real time is decreased. Therefore, it should be considered that there are two counteractive effects

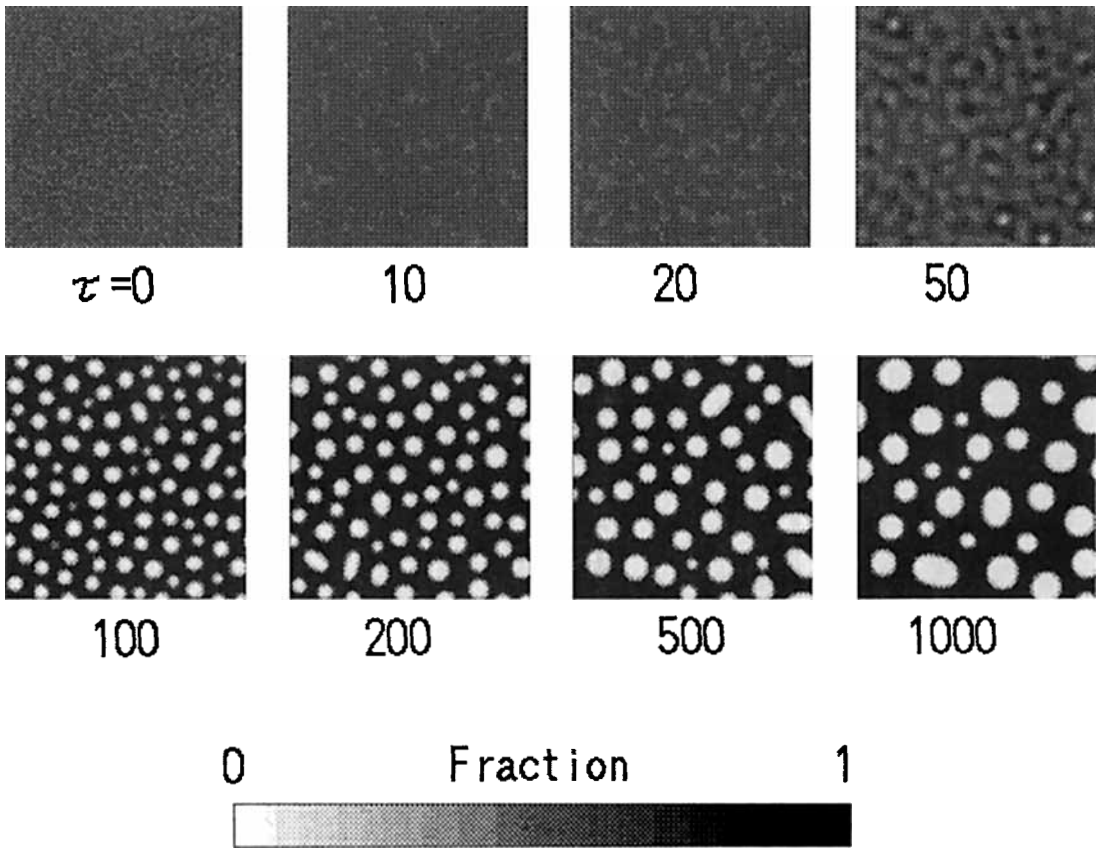

Figure 3 Phase structures during phase separation for volume fraction 0.7 in dimensionless scale.

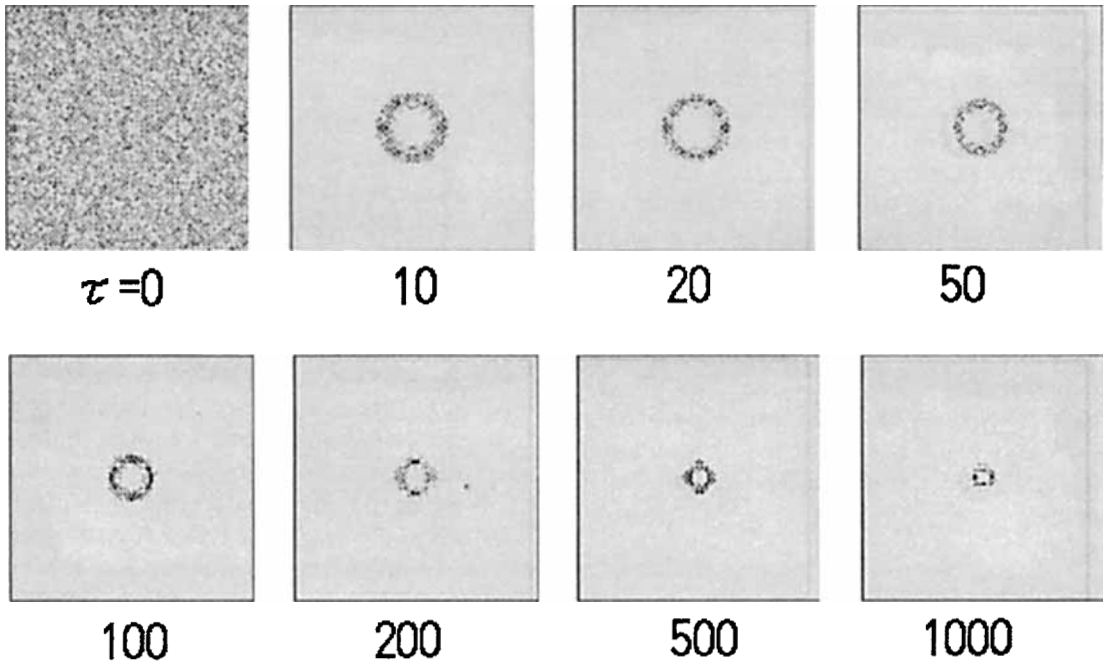

Figure 4 Fourier transformed profiles of phase structures for volume fraction 0.5.

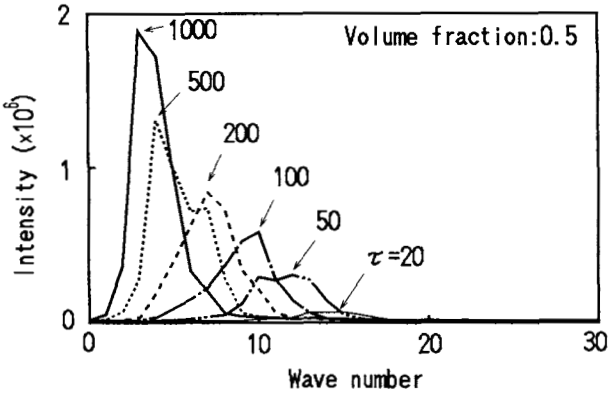

Figure 5 Evolution of power spectra during phase separation.

of the number of segments on the phase separation in the real time.

The solubility parameter dramatically changes the evolution of Φ, as shown in Figure 9. As the difference of the solubility parameter, $\Delta\delta$, decreases, the phase separation time increases. If $\Delta\delta \leqq 0.2$ (cal/cm^3)$^{1/2}$, the phase separation is not caused before $t^* = 10{,}000$. For $\Delta\delta = 1.5$, the phase separation is caused before $t^* = 10$, which is the earliest time among the calculation conditions. Φ increases with time, following that it becomes constant after $t^* = 100$. This is due to the fact that the morphology does not change any more after phase separation with time. Phase structures for $\Delta\delta = 0.5$, 1.0, and 1.5 are shown in Figure 10. For $\Delta\delta = 0.5$, the phase separation does not occur at $t^* = 100$, when the phase structure is clear for the other conditions but the domain size at $t^* = 1{,}000$ is almost the same as that for $\Delta\delta = 1.0$. For $\Delta\delta = 1.5$, a very fine structure appears at $t^* = 10$ and coarsens a little at $t^* = 100$, but after that, the fine structure has no more change.

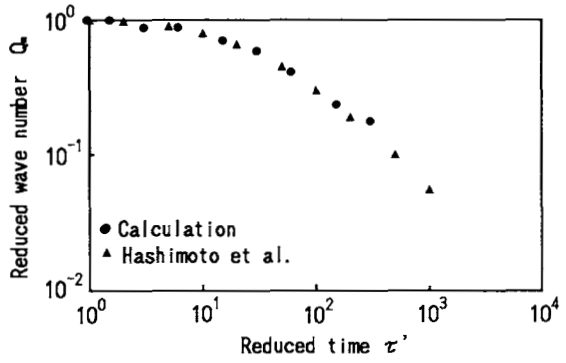

Figure 6 Comparison of calculated results with experimental one on evolution reduced wave number for volume fraction 0.5.

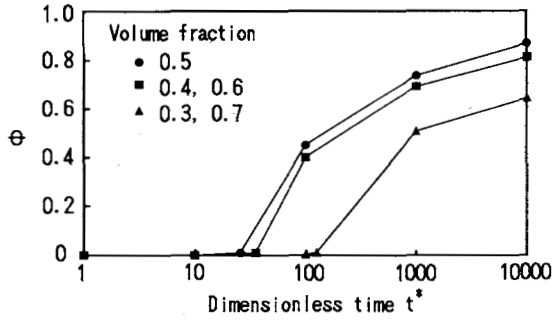

Figure 7 Effect of the volume fraction of polymer 2 on Φ.

The solubility parameter seems to have two effects on the phase separation. One is the acceleration of phase separation and the other is the restriction of structure coarsening.

DISCUSSION

The interfacial tension, which is important to discuss the phase structure, is an increment of the free energy per unit area described as follows:[17]

$$\sigma = (1/3)k_B T K^{1/2}(2b)^{3/2}/u \qquad (28)$$

Because the calculation was made under isothermal condition, $(1/3)k_B T$ is constant. Then σ^* is defined as:

$$\sigma^* = [3/(k_B T)]\sigma \qquad (29)$$

Moreover, the spinodal decomposition is caused when the following relation is satisfied:

$$\varepsilon = -b + 3u\phi_a^2 < 0 \qquad (30)$$

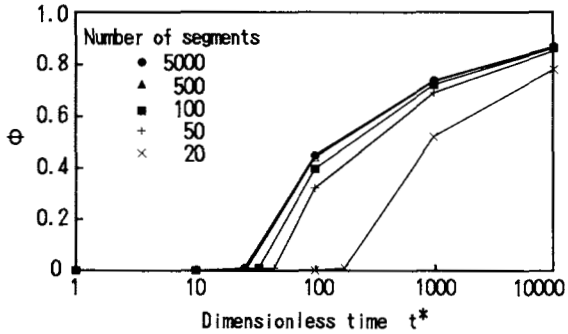

Figure 8 Effect of the number of segments of polymer 2 on Φ.

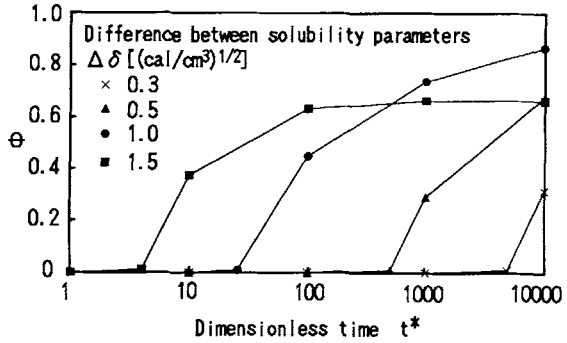

Figure 9 Effect of the difference between solubility parameters on Φ.

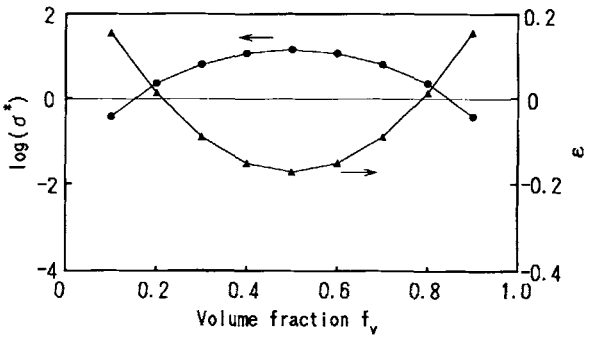

Figure 11 Plots of log σ^* and ε vs. the volume fraction.

where, ϕ_a is the average order parameter.

Using eqs. (29) and (30), σ^* and ε were estimated for calculation conditions. They are plotted vs. volume fraction f_v, as shown in Figure 11. The interfacial tension is maximum at a volume fraction of 0.5 and decreases with both increasing and decreasing volume fraction from 0.5. The change of ε shows

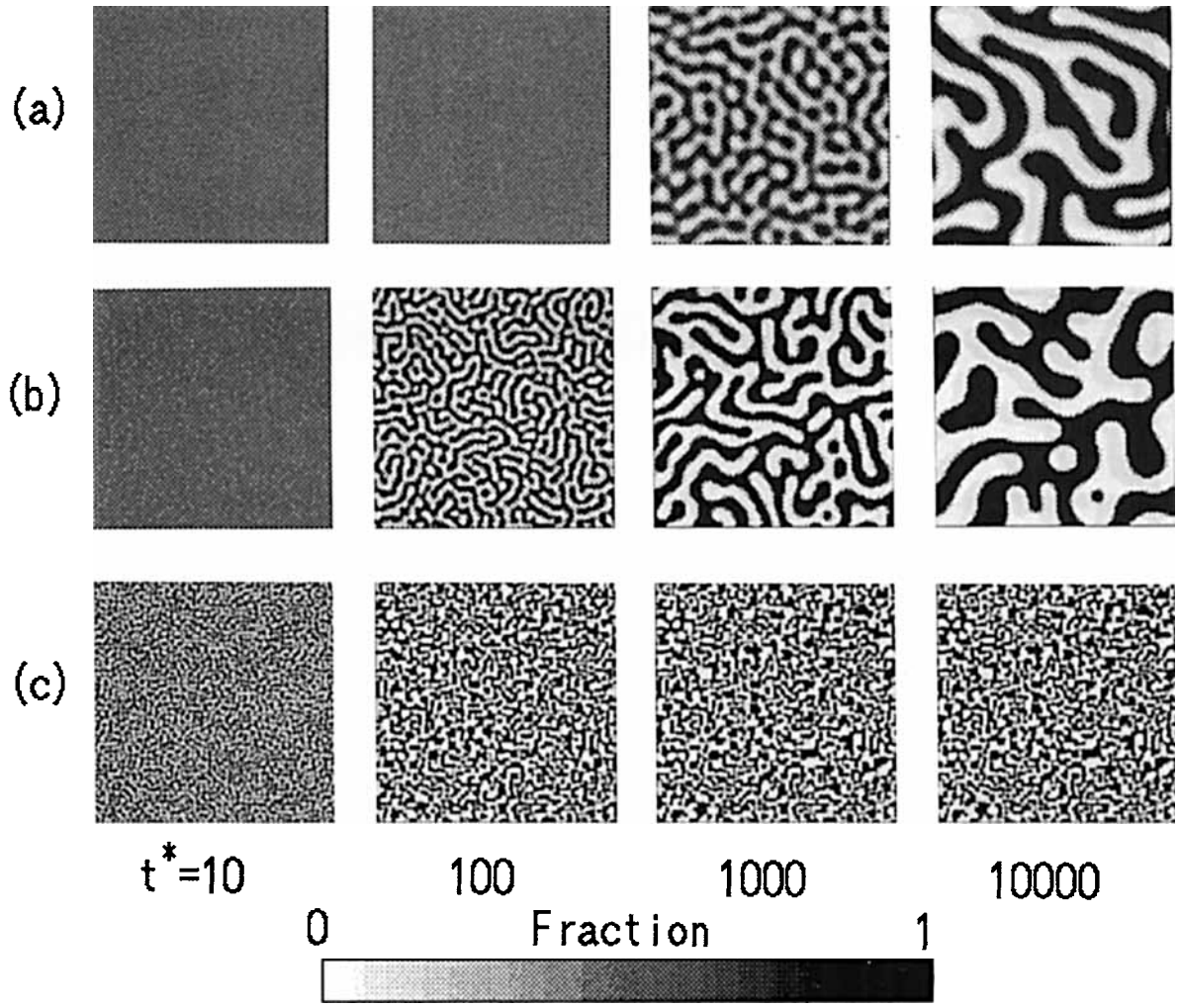

Figure 10 Phase structures during phase separation for (a) $\Delta\delta = 0.5$, (b) $\Delta\delta = 1.0$, and (c) $\Delta\delta = 1.5$.

the opposite tendency to that of σ^*. The plot of ε shows that the phase separation is caused in the volume fraction range of 0.3 to 0.7 because ε is negative. On the other hand, when $f_v \leqq 0.2$ or $0.8 \leqq f_v$, the phase will not separate because $\varepsilon > 0$. The volume fraction to prevent phase separation agrees with that obtained by the previous numerical simulation. Figure 12 shows σ^* and ε vs. the number of segments N. As the number of segments decreases, the interfacial tension is decreased until nearly 50 and then dramatically drops after that. ε is, however, almost constant until 100 and then increases but remains being negative. The change of ε corresponds to the change of the phase separation time owing to number of segments in the numerical simulation. Finally, Figure 13 shows the effect of the solubility parameter on σ^* and ε. With decreasing the difference between solubility parameters $\Delta\delta$, the interfacial tension decreases and ε increases approaching zero. If $\Delta\delta$ is very small, the phase separation may not appear for a long time.

Summarizing the above three figures, the relation between σ^* and ε is shown in Figure 14. As is evident from the figure, large interfacial tension cause the phase separation. We can reduce the interfacial tension by changing the volume fraction, number of segments, and solubility parameter. However, the occurrence of the phase separation cannot be predicted only from the interfacial tension. It is noted that the factor that makes ε positive is only the volume fraction. This corresponds with the idea of a phase diagram. For the number of segments and solubility parameter, ε only approaches zero with negative sign as interfacial tension decreases. Then, ε indicates that the phase separation is not prevented by changing the number of segments and solubility parameters. On the other hand, the phase separation is vanished with decreasing them, as described in the previous simulation. This discrepancy is due to the difference of time scale. ε is discussed in infinite time but the simulation in finite. If a computer could be run infinitely, the phase separation may be caused anytime also in simulations, as ε indicates. It was said that the computer simulation is useful to predict the occurrence of the phase separation within a given time and the phase structure after that.

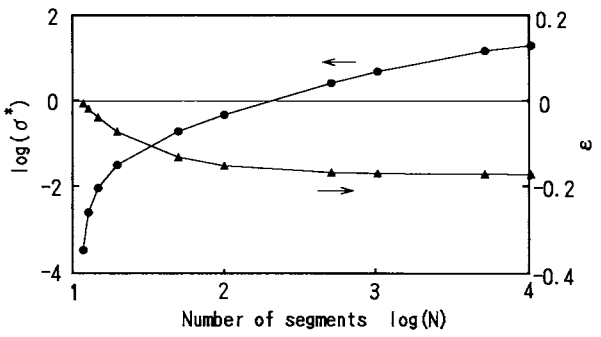

Figure 12 Plots of log σ^* and ε vs. log-number of segments.

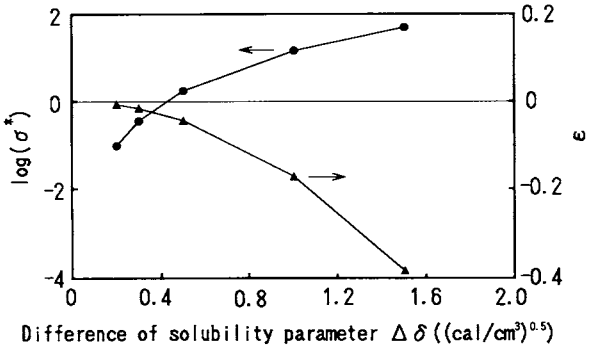

Figure 13 Plots of log σ^* and ε vs. the difference of solubility parameters.

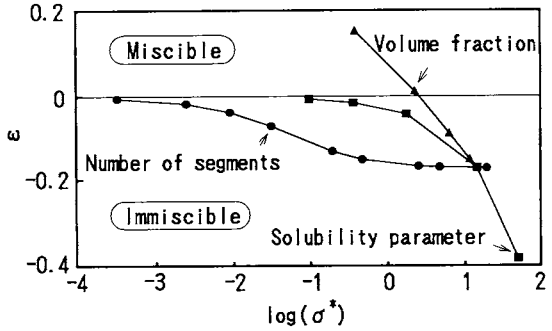

Figure 14 Relation between ε and log σ^*.

CONCLUSIONS

In this article the phase separation of binary polymer mixtures was numerically simulated by solving the time-dependent Langevin equation with Flory–Huggins free energy in two dimensions using a finite difference method. The amplification of concentration fluctuation and the structure coarsening during phase separation process were calculated. To verify the computation, the evolution of the wave number, at which the power spectrum shows peak, was evaluated from the calculated phase structure by the fast Fourier transformation and then was compared with light scattering results reported in the literature. As a result, the calculation was proved from good agreement between them.

Then, changing volume fraction, number of segments, and solubility parameter of one of the components, their effects on phase separation and structure were numerically investigated. The phase separation time, at which the statistic dispersion of order parameter began to rise rapidly from nearly zero, decreased with deviating volume fraction from 0.5 and with decreasing number of segments and difference between solubility parameters. The difference between solubility parameters had the largest influence on the phase separation time among them and had two effects, the acceleration of phase separation and the restriction of structure coarsening. The effect of the polymer characters was qualitatively explained by the change of interfacial tension.

REFERENCES

1. H. Tanaka, T. Hayashi, and T. Nishi, *J. Appl. Phys.*, **59,** 3627 (1986).
2. H. L. Snyder and P. Meakin, *J. Polym. Sci.*, **73,** 217 (1985).
3. T. Hashimoto, M. Itakura, and N. Shimidzu, *J. Chem. Phys.*, **85,** 6773 (1986).
4. A. Levy, S. Reich, and P. Meakin, *Phys. Lett.*, **87A,** 248 (1982).
5. A. Baumgärtner and D. W. Heermann, *Polymer,* **27,** 1777 (1986).
6. A. Sariban and K. Binder, *J. Chem. Phys.*, **86,** 5859 (1987).
7. P. Cifra, F. E. Karasz, and W. J. Macknight, *J. Polym. Sci. B,* **26,** 2379 (1988).
8. J. W. Cahn and J. E. Hilliard, *J. Chem. Phys.*, **28,** 258 (1958).
9. H. E. Cook, *Acta. Metall.*, **18,** 297 (1970).
10. R. Petschek and H. Metiu, *J. Chem. Phys.*, **79,** 3443 (1983).
11. A. Chakrabarti, R. Toral, and J. Gunton, *Phys. Rev. B,* **39,** 4386 (1989).
12. M. V. Ariyapadi, E. B. Nauman, and J. W. Haus, in *Computer Simulation of Polymers,* R. J. Roe, Ed., Prentice–Hall, Englewood Cliffs, NJ, 1991, p. 374.
13. Y. Chen, K. Solc, and G. T. Caneba, *Polym. Eng. Sci.*, **33,** 1033 (1993).
14. P. G. de Gennes, *J. Chem. Phys.*, **72,** 4756 (1980).
15. K. Binder, *J. Chem. Phys.*, **79,** 6387 (1983).
16. J. Brandrup and E. H. Immergut, Eds., *Polymer Handbook Third Edition,* John Wiley & Sons, New York, 1989.
17. M. Doi and A. Onuki, *Polymer Physics and Dynamics of Phase Transition,* Iwanami, Tokyo, 1992, p. 148.

Received November 17, 1994
Accepted January 19, 1995